Stanford Exploration Project, Report 129, May 6, 2007, pages 43–56

Two-way vs. one-way: Understanding the approximations

Alejandro A. Valenciano

ABSTRACT

The one-way wave-equation approximation has a big impact on migration, modeling, and wave-equation inversion. That is why Amplitude vs. subsurface-offset (AVO), and amplitude vs. reflection angle (AVA) responses of the migration of a two-way and a one-way modeled datasets show different illumination patterns. Deconvolution by the one-way wave-equation Hessian can be use to account for the illumination problem. But the approximations used to compute the Hessian have an impact on how effectively the medium AVO and AVA is recover by the inversion.

INTRODUCTION

The dream of an explorationist is to be able to carry on AVO or AVA attributes analysis in areas with poor illumination. But the quality of the images that a state of the art migration can produce is not good enough for that purpose. One way to improve the image is to use an inversion formalism introduced by Tarantola (1987) to solve geophysical imaging problems. This procedure computes an image by convolving the migration result with the inverse of the Hessian matrix.

When the dimensions of the problem get large, the explicit calculation of the Hessian matrix and its inverse becomes unfeasible. That is why Valenciano and Biondi (2004) and Valenciano et al. (2006) proposed the following approximations: (1) to compute the one way wave equation Green functions from the surface to the target (or vice versa), to reduce the size of the problem; (2) to compute the Hessian, exploiting its sparse structure; and (3) to compute the inverse image following an iterative inversion scheme. The last item renders unnecessary an explicit computation of the inverse of the Hessian matrix. For efficiency reasons the Green's functions necessary to compute the Hessian are computed by means of a one-way wave-equation extrapolator.

In this paper I study the impact of the one-way wave-equation approximation to the wave propagation in: migration, modeling, and wave-equation inversion. I illustrate the differences between two-way and one-way data modeling, and the migration of two-way and one-way modeled data.

I also show how the approximations used to compute the Hessian have an impact on the recovery of the medium AVO and AVA response. This is done by comparing the inversion of

the two-way modeled TRIP data, a one-way modeled data (equivalent to the use of the full Hessian), and a one-way modeled data using an approximated Hessian.

LINEAR LEAST-SQUARES INVERSION

Tarantola (1987) formalizes the geophysical inverse problem by providing a theoretical approach to compensate for experimental deficiencies (e.g., acquisition geometry, complex overburden), while being consistent with the acquired data. His approach can be summarized as follows: given a linear modeling operator $\mathbf{L}$, compute synthetic data $\mathbf{d}$ using $\mathbf{d} = \mathbf{L}\mathbf{m}$ where $\mathbf{m}$ is a reflectivity model. Given the recorded data $\mathbf{d}_{obs}$, a quadratic cost function,

$$S(\mathbf{m}) = \|\mathbf{d} - \mathbf{d}_{obs}\|^2 = \|\mathbf{L}\mathbf{m} - \mathbf{d}_{obs}\|^2, \tag{1}$$

is formed. The reflectivity model $\hat{\mathbf{m}}$ that minimizes $S(\mathbf{m})$ is given by the following:

$$\hat{\mathbf{m}} = (\mathbf{L}'\mathbf{L})^{-1}\mathbf{L}'\mathbf{d}_{obs} = \mathbf{H}^{-1}\mathbf{m}_{mig}, \tag{2}$$

where $\mathbf{L}'$ (migration operator) is the adjoint of the linear modeling operator $\mathbf{L}$, $\mathbf{m}_{mig}$ is the migration image, and $\mathbf{H} = \mathbf{L}'\mathbf{L}$ is the Hessian of $S(\mathbf{m})$.

The main difficulty with this approach is the explicit calculation of the inverse Hessian. In practice, it is more feasible to compute the least-squares inverse image as the solution of the linear system,

$$\mathbf{H}\hat{\mathbf{m}} = \mathbf{m}_{mig}, \tag{3}$$

by using an iterative inversion algorithm.

Equation 3 states that if we convolve the Hessian matrix $\mathbf{H}$ with a perfect model we should obtain the migration result ("Hessian impulse response"). In the next section we will study the approximations involved in the computation of the Hessian matrix, and will try to understand how far the "Hessian impulse response" computed using the approximated Hessian (from equation 3) is from the real migration result.

Subsurface-offset Hessian

Valenciano et al. (2006) define the zero subsurface-offset domain Hessian by using the adjoint of the zero subsurface-offset domain migration as the modeling operator $\mathbf{L}$. Then the zero-subsurface-offset inverse image can be estimated as the solution of a non-stationary least-squares filtering problem, using an iterative inversion algorithm (Valenciano et al., 2006).

The subsurface-offset Hessian was defined by Valenciano and Biondi (2006). The definition can be summarized as follows.

The prestack migration image (subsurface-offset domain) for a group of shots positioned at $\mathbf{x}_s = (x_s, y_s, 0)$ and a group of receivers positioned at $\mathbf{x}_r = (x_r, y_r, 0)$ can be given by the

adjoint of a linear operator $\mathbf{L}$ acting on the data-space $\mathbf{d}(\mathbf{x}_s,\mathbf{x}_r;\omega)$ as

$$\begin{aligned}\mathbf{m}(\mathbf{x},\mathbf{h}) &= \mathbf{L}'\mathbf{d}(\mathbf{x}_s,\mathbf{x}_r;\omega) \\ &= \sum_{\omega}\sum_{\mathbf{x}_s}\sum_{\mathbf{x}_r}\mathbf{f}(\omega)\mathbf{G}'(\mathbf{x}-\mathbf{h},\mathbf{x}_s;\omega)\mathbf{G}'(\mathbf{x}+\mathbf{h},\mathbf{x}_r;\omega)\sum_{\mathbf{h}}{}'\sum_{\mathbf{x}}{}'\mathbf{d}(\mathbf{x}_s,\mathbf{x}_r;\omega),\end{aligned} \tag{4}$$

where $\mathbf{G}(\mathbf{x},\mathbf{x}_s;\omega)$ and $\mathbf{G}(\mathbf{x},\mathbf{x}_r;\omega)$ are respectively the Green's functions from the shot position $\mathbf{x}_s$ and from the receiver position $\mathbf{x}_r$ to a point in the model space $\mathbf{x}$, $\mathbf{f}(\omega)$ is the source wavelet, and $\mathbf{h}=(h_x,h_y)$ is the subsurface-offset. The symbols $\sum_{\mathbf{h}}'$ and $\sum_{\mathbf{x}}'$ are spray operators (adjoint of the sum) in the subsurface-offset and physical space dimensions $\mathbf{x}=(x,y,z)$, respectively. The Green's functions are computed by means of the one-way wave-equation.

The synthetic data can be modeled (as the adjoint of equation 4) by the linear operator $\mathbf{L}$ acting on the model space $\mathbf{m}(\mathbf{x},\mathbf{h})$

$$\begin{aligned}\mathbf{d}(\mathbf{x}_s,\mathbf{x}_r;\omega) &= \mathbf{L}\mathbf{m}(\mathbf{x},\mathbf{h}) \\ &= \sum_{\mathbf{x}}\sum_{\mathbf{h}}\mathbf{G}(\mathbf{x}+\mathbf{h},\mathbf{x}_r;\omega)\mathbf{f}(\omega)\mathbf{G}(\mathbf{x}-\mathbf{h},\mathbf{x}_s;\omega)\sum_{\mathbf{x}_r}{}'\sum_{\mathbf{x}_s}{}'\sum_{\omega}{}'\mathbf{m}(\mathbf{x},\mathbf{h}),\end{aligned} \tag{5}$$

where the symbols $\sum_{\mathbf{x}_r}{}'$, $\sum_{\mathbf{x}_s}{}'$, and $\sum_{\omega}{}'$ are spray operators in the shot, receiver, and frequency dimensions, respectively.

The second derivative of the quadratic cost function with respect to the model parameters is the subsurface-offset Hessian:

$$\begin{aligned}\mathbf{H}(\mathbf{x},\mathbf{h};\mathbf{x}',\mathbf{h}') = \sum_{\omega}\mathbf{f}(\omega)^2\sum_{\mathbf{x}_s}\mathbf{G}'(\mathbf{x}-\mathbf{h},\mathbf{x}_s;\omega)\mathbf{G}(\mathbf{x}'-\mathbf{h}',\mathbf{x}_s;\omega) \\ \times\sum_{\mathbf{x}_r}\mathbf{G}'(\mathbf{x}+\mathbf{h},\mathbf{x}_r;\omega)\mathbf{G}(\mathbf{x}'+\mathbf{h}',\mathbf{x}_r;\omega),\end{aligned} \tag{6}$$

where $(\mathbf{x}',\mathbf{h}')$ are the off-diagonal terms of the Hessian matrix.

An approximation to the full subsurface-offset Hessian involves computing only the off-diagonal terms at close to the diagonal (Valenciano and Biondi, 2006).

$$\begin{aligned}\mathbf{H}(\mathbf{x},\mathbf{h};\mathbf{x}+\mathbf{a},\mathbf{h}') = \sum_{\omega}\mathbf{f}(\omega)^2\sum_{\mathbf{x}_s}\mathbf{G}'(\mathbf{x}-\mathbf{h},\mathbf{x}_s;\omega)\mathbf{G}(\mathbf{x}+\mathbf{a}-\mathbf{h}',\mathbf{x}_s;\omega) \\ \times\sum_{\mathbf{x}_r}\mathbf{G}'(\mathbf{x}+\mathbf{h},\mathbf{x}_r;\omega)\mathbf{G}(\mathbf{x}+\mathbf{a}+\mathbf{h}',\mathbf{x}_r;\omega),\end{aligned} \tag{7}$$

where $\mathbf{a}=(a_x,a_y,a_z)$ are the off-diagonal coefficients. The impact of this approximation will be evaluated in the following sections.

Data fitting goal

In this paper I do not use any regularization to solve the linear system in equation 3, since the objective of the study was to find out how well the Hessian operator could fit the different

kind of data. Having regularization could obscure the results. However, in areas of poor illumination, this problem will have a large null space. The null space is partially caused by the fact that our survey can not have infinite extents and infinitely dense source and receiver grids. Any noise that exists within the null space can grow with each iteration until the problem becomes unstable.

The inversion was carried out in the subsurface-offset domain. The fitting goal used was

$$\mathbf{H}(\mathbf{x},\mathbf{h};\mathbf{x}',\mathbf{h}')\hat{\mathbf{m}}(\mathbf{x},\mathbf{h}) - \mathbf{m}_{mig}(\mathbf{x},\mathbf{h}) \quad \approx \quad 0, \tag{8}$$

In the next sections I compare the numerical solution of the inversion problems stated in equation 8 in the imaging of the TRIP synthetic dataset.

TWO-WAY VS. ONE-WAY MODELING

For efficiency reasons the Green's functions in equations 4, 5, and 6 are computed by means of a one-way wave-equation extrapolator. No upgoing energy can be modeled by following this approach, since the evanescent energy is usually damped (Claerbout, 1985). This makes the one-way propagator act as a dip filter depending on the velocity model (from the dispersion relation, $\frac{\omega^2}{v^2} < \mathbf{k}^2$). Also, the conventional one-way wave-equation does not model accurately the the amplitude behavior with the angle of propagation (Zhang et al., 2005). Another problem arises when the velocity varies laterally, then getting energy to accurately propagate close to 90° is a big challenge.

The previous limitations of the one-way modeling can be mitigated by getting sophisticated when implementing the extrapolator. The dip filter effect should be reduced by including the Jacobian of the change of variable from ω to k_z (Sava and Biondi, 2001), thus making $\mathbf{L}$ closer to be unitary. To properly model the amplitude behavior with the angle of propagation, Zhang et al. (2005) proposed using a modified one-way wave-equation who's solution match the Kirchhoff inversion solution. The effect caused by the lateral variation of the velocity can also be mitigated by using better approximations of the square root operator.

For the example presented in this paper I used the conventional one-way wave equation (Claerbout, 1985). I did not include the Jacobian, and approximated the square root operator with Split Step Fourier plus interpolation (PSPI).

NUMERICAL RESULTS

Modeling

The TRIP synthetic dataset was created from a model with a constant-reflectivity flat reflector lying beneath a Gaussian low velocity anomaly (Figure 1). The data was modeled with the following acquisition geometry: the shots and receivers were positioned every 10 m on the interval $\mathbf{x} = [-2.0, 2.0]$ km .

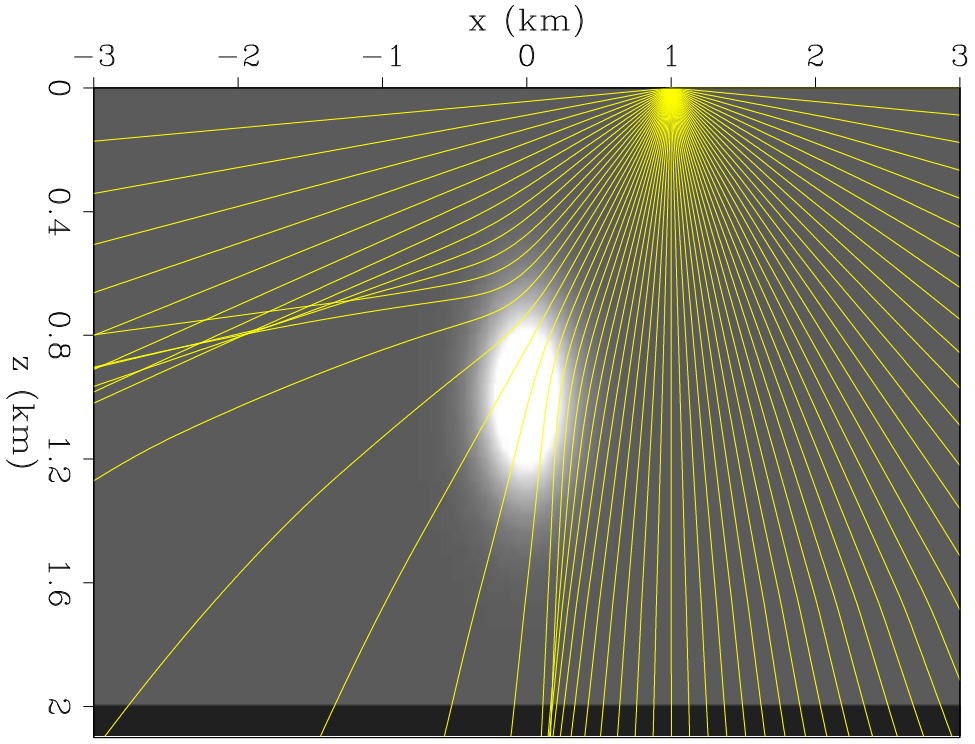

Figure 1: Gaussian anomaly velocity model with overlay rays showing the uneven illumination of the reflector. alejandro1-rays [ER]

The Gaussian anomaly distorts the direction in which the energy is propagated (from small to high angles) and it also makes the velocity change with x position, thus the effect of using one-way vs. two-way modeling should be noticeable. One important difference between these two data sets is the assumed AVA of the flat reflector. I assumed a constant AVA when modeling the one-way data with equation 5. Conversely, a AVA corresponding to a constant density is implicit in the TRIP two-way finite-differences modeling code.

Figure 2 shows a comparison of the two-way (Figures 2a, 2c) modeled data provided by TRIP vs. the one-way (Figures 2b, 2d) modeled using equation 5. The first row correspond to a shot located at $x = -2$ km, and the bottom row corresponds to a shot located at $x = 1$ km.

The main differences (besides the artifact in the two-way modeling with linear moveout) can be spotted in the top row. The one-way modeled data (Figure 2a) shows a decay of the amplitude with offset (compare with Figure 2b) that could be related to the errors in the amplitude (absence of the Jacobian) in the one-way extrapolator. There is also an overturning event arriving at far offset (Figure 2b), which is impossible to model with the one-way extrapolator. Besides the AVO differences (dynamic) a very good agreement of the kinematics can be observed.

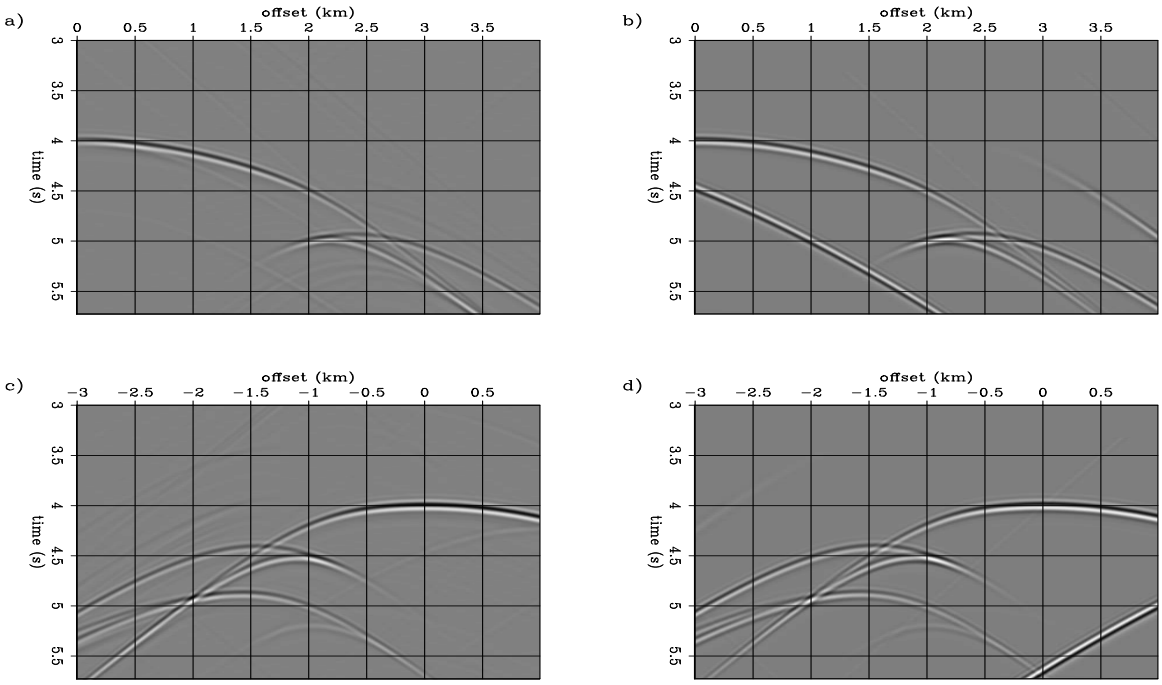

Figure 2: Comparison of the two-way (b,d) modeled data provided by TRIP vs. the one-way (a,c) modeled using equation 5. The top row shows the data from a shot located at $x = -2$ km, and the bottom row corresponds to a shot located at $x = 1$ km. alejandro1-compare [CR,M]

Migration

The next step is to compare the subsurface-offset migration results from the two different data sets. Figure 3 shows a comparison the two-way (3a) vs. the one-way modeled data (3b) migrations in the subsurface-offset domain. The results are comparable in terms of resolution, but the amplitudes show a different behavior. This is something to expect from the data differences in AVO behavior (Figure 2). Even though the images shown in Figure 3 are in the sub-surface offset domain, we can see how different they are going to be when transformed to reflection angle by using Sava and Fomel (2003) transformation.

Figure 4 shows a comparison the two-way (Figure 4a) vs. the one-way modeled data (Figure 4b) migrations in the reflection angle domain. This result is obtained after applying an offset to angle transformation to the images in Figure 3. Notice the difference between the illumination patterns in the images. As we discussed in the modeling subsection the images in Figure 4a and Figure 4b should have different AVA responses. But, from inspecting the figures we can see that they are not that far apart. For most of the a x positions the angle range illumination is the same, being different in intensity. I will discuss the impact of this on the recovery of the AVA in the Inversion subsection.

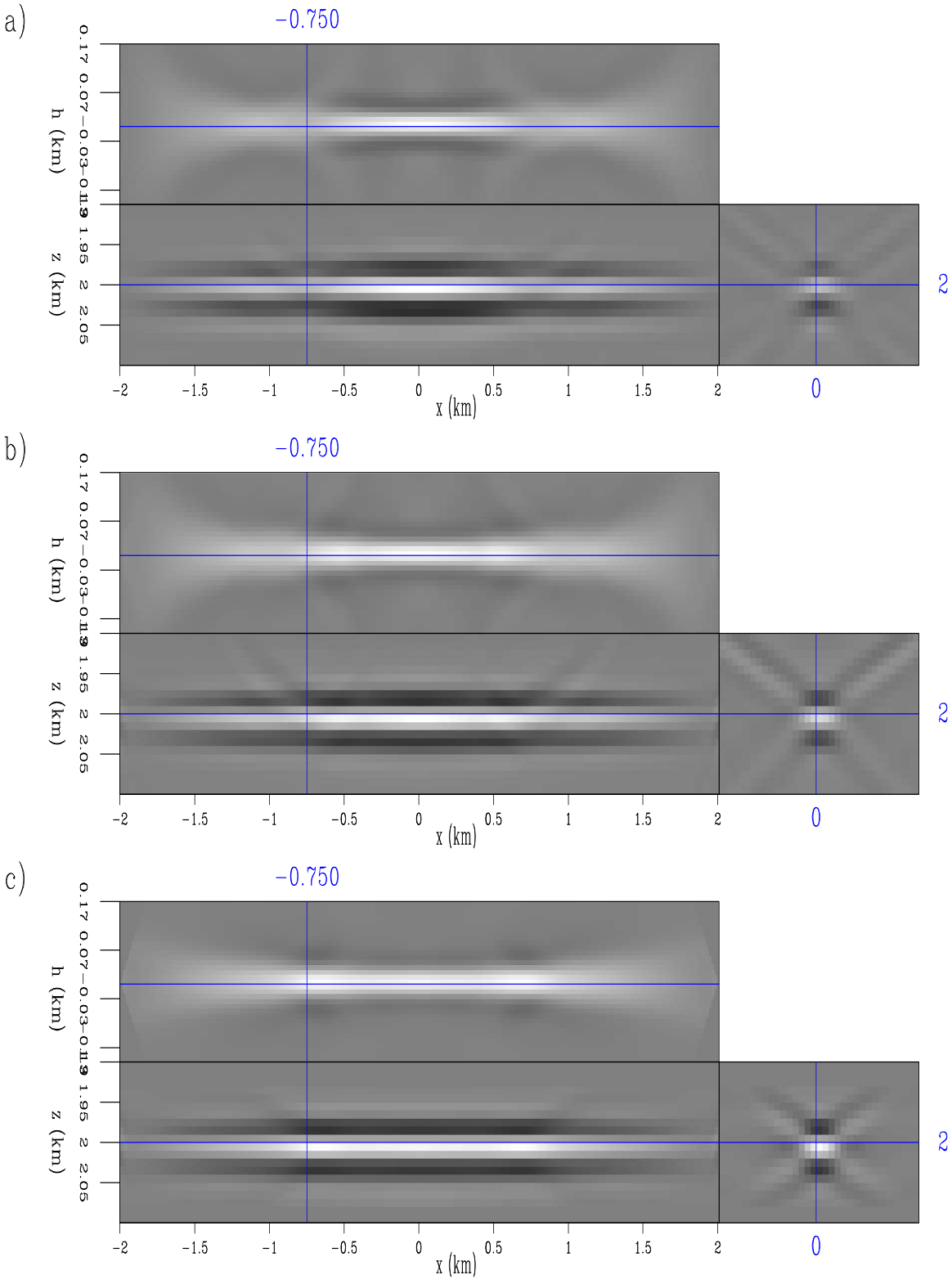

Figure 3: Comparison of the migration results in subsurface-offset domain of the two-way (a) vs. the one-way modeled data (b), and vs. the migration "Hessian impulse response" (c) (from equation 3) alejandro1-compare_mig1 [CR,M]

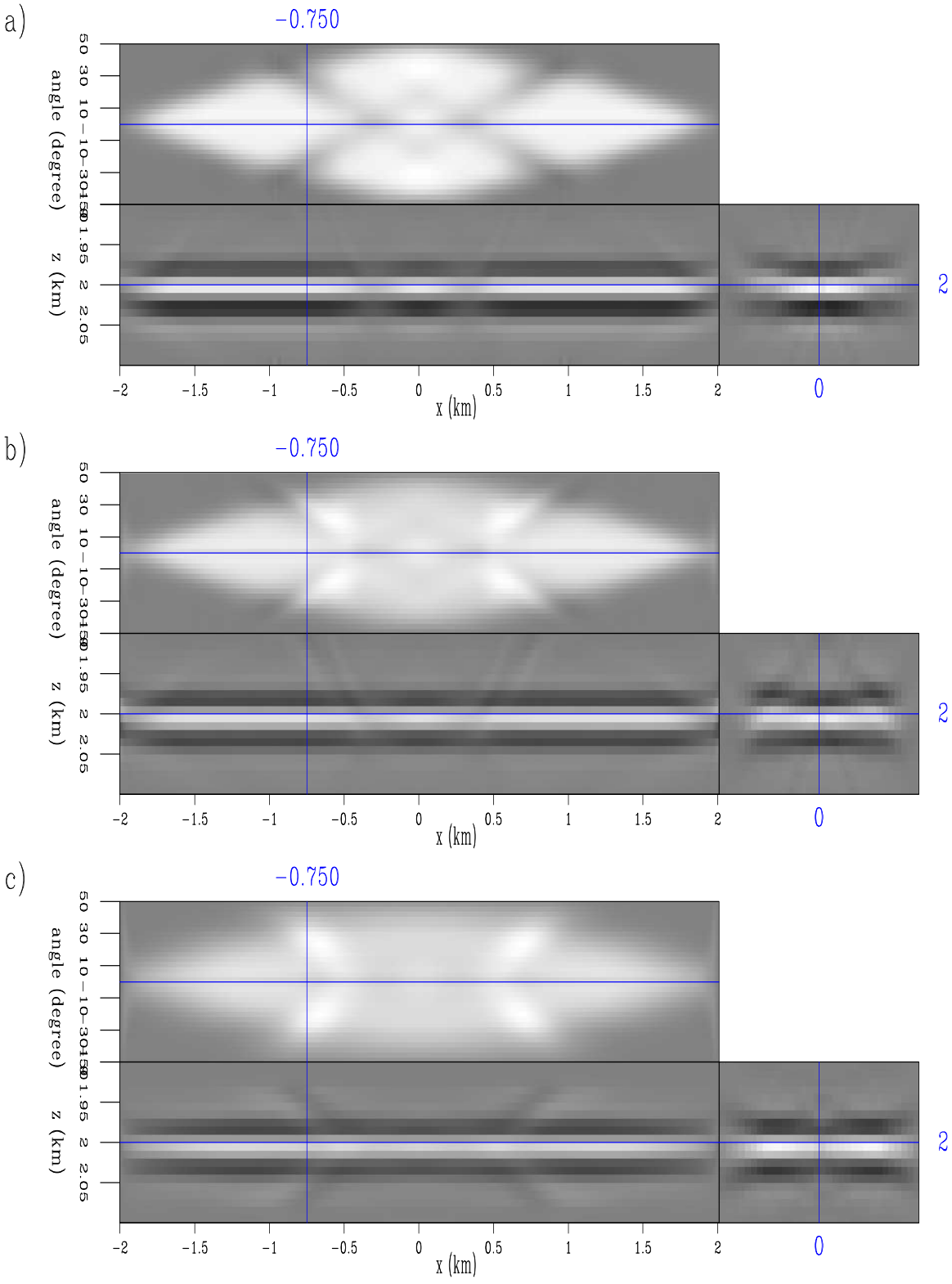

Figure 4: Comparison of the migration results in reflection angle of the two-way (a) vs. the one-way modeled data (b), and vs. the migration "Hessian impulse response" (c) (from equation 3) alejandro1-compare_mig2 [CR,M]

Migration vs. "Hessian impulse response"

Another important comparison is the between the the one-way modeled data migration (Figures 3b and 4b) and the migration "Hessian impulse response" (Figures 3c and 4c). This two results should have been identical if all the off-diagonal terms of the Hessian matrix would have been computed (equation 7) to obtain Figures 3c. In the modeling of the one-way data all the off-diagonal elements of the Hessian matrix are implicitly computed. To obtain Figure 3c only ($a_x = 15 \times a_z = 15 \times h' = 32$) off-diagonal elements of the Hessian matrix were computed.

The two results are very similar at small offsets, but at far subsurface-offset the migration "Hessian impulse response" (Figure 3c) amplitudes are washed out. That might indicate the need of computing more off-diagonal coefficients in the (x, z) dimensions (a_x, a_z), probably the same number off subsurface-offsets. The angle migration "Hessian impulse response" differs at higher angles to the angle one-way modeled data migration, a result that is the consequence of the washed out amplitudes at far subsurface-offset "Hessian impulse response".

An important feature to notice when comparing Figures 4a, 4b, and 4c is that some places with low illumination in Figure 4a, have high illumination in Figure 4b, and Figure 4c. In those places the deconvolution by the one-way wave-equation Hessian will not recover the correct amplitudes. Thus the AVA signature will be affected.

Inversion

Deconvolution by the one-way wave-equation Hessian can be use to account for the illumination problem caused by the low velocity Gaussian anomaly (Figure 4). To understand the effect of using one-way wave-equation Green functions in the Hessian computation, I compare the inversion of the: two-way modeled data (Figures 5a, and 6a), the one-way modeled data (Figures 5b, and 6b), and the migration "Hessian impulse response" (Figures 5c, and 6c). The images in Figure 6 are the result of applying an offset to angle transformation to the images in Figure 5.

The first thing to notice is that in the case in that the same operator was used for the modeling and for the inversion ("Hessian impulse response", Figures 5c, and 6c) the deconvolution by the Hessian gives a almost perfect result. See how the energy in the subsurface-offset dimension concentrates around zero subsurface-offset (Figure 5c), and by consequence the more uniform angle coverage (Figure 6c) compare to the migration results in Figures 3c and 4c.

The second best result is obtained for the one-way modeled data inversion (Figures 5b, and 6b). Here the operators used for the modeling (implicitly) and the operator used for the inversion (explicitly) differ, since not all the of off-diagonal elements of the Hessian were computed. Nevertheless, there is an improvement in the AVA uniformity (expected from modeling) in most of the x positions. Especially at the center of the model.

The result of the two-way modeled data inversion (Figures 5a, and 6a) is the one showing less improvements. Nevertheless, there are several x positions where the AVA looks less

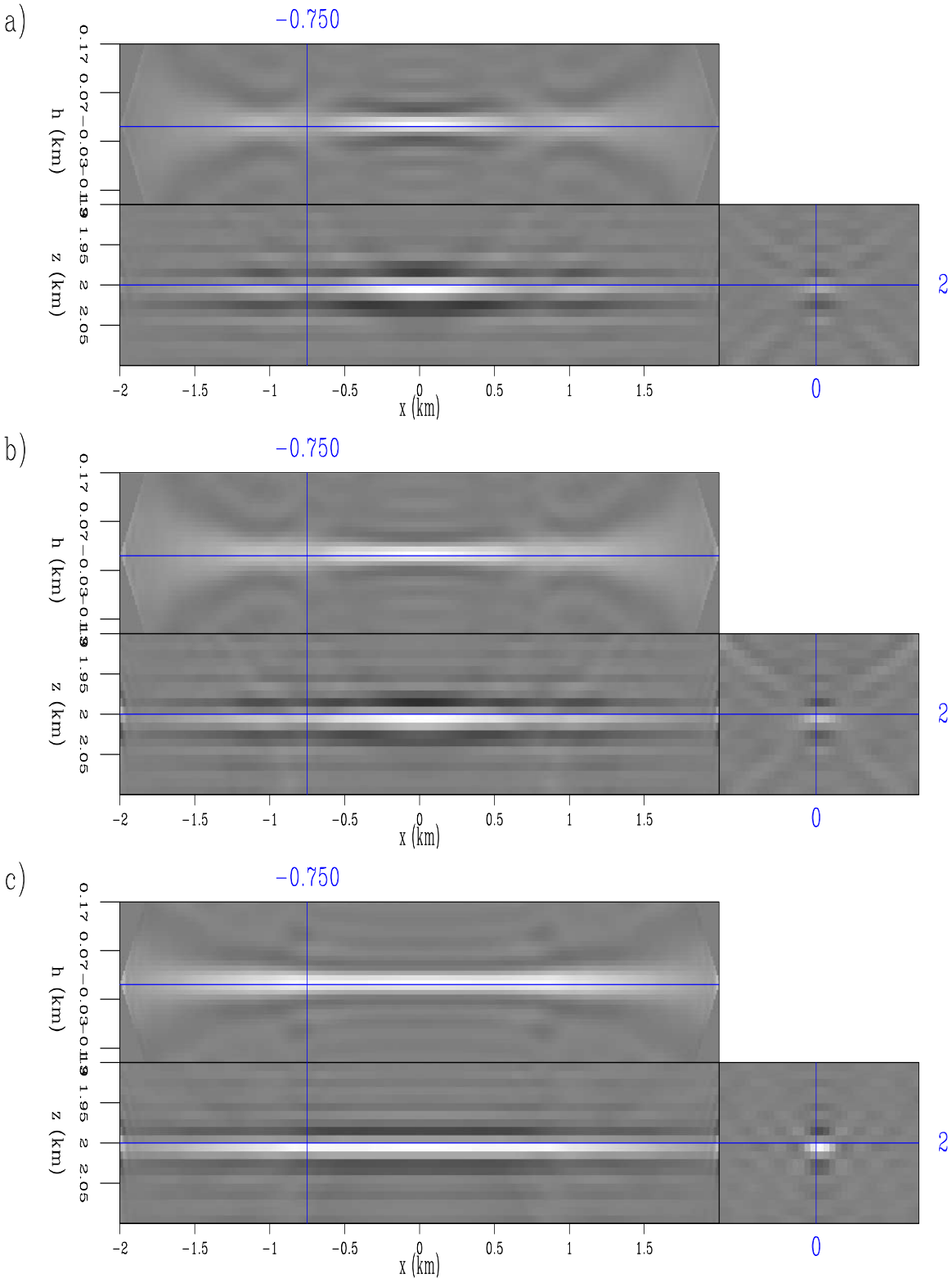

Figure 5: Comparison of the inversion results in reflection angle of the two-way (a) vs. the one-way modeled data (b), and vs. the migration "Hessian impulse response" (c) (from equation 3) alejandro1-compare_inv1 [CR,M]

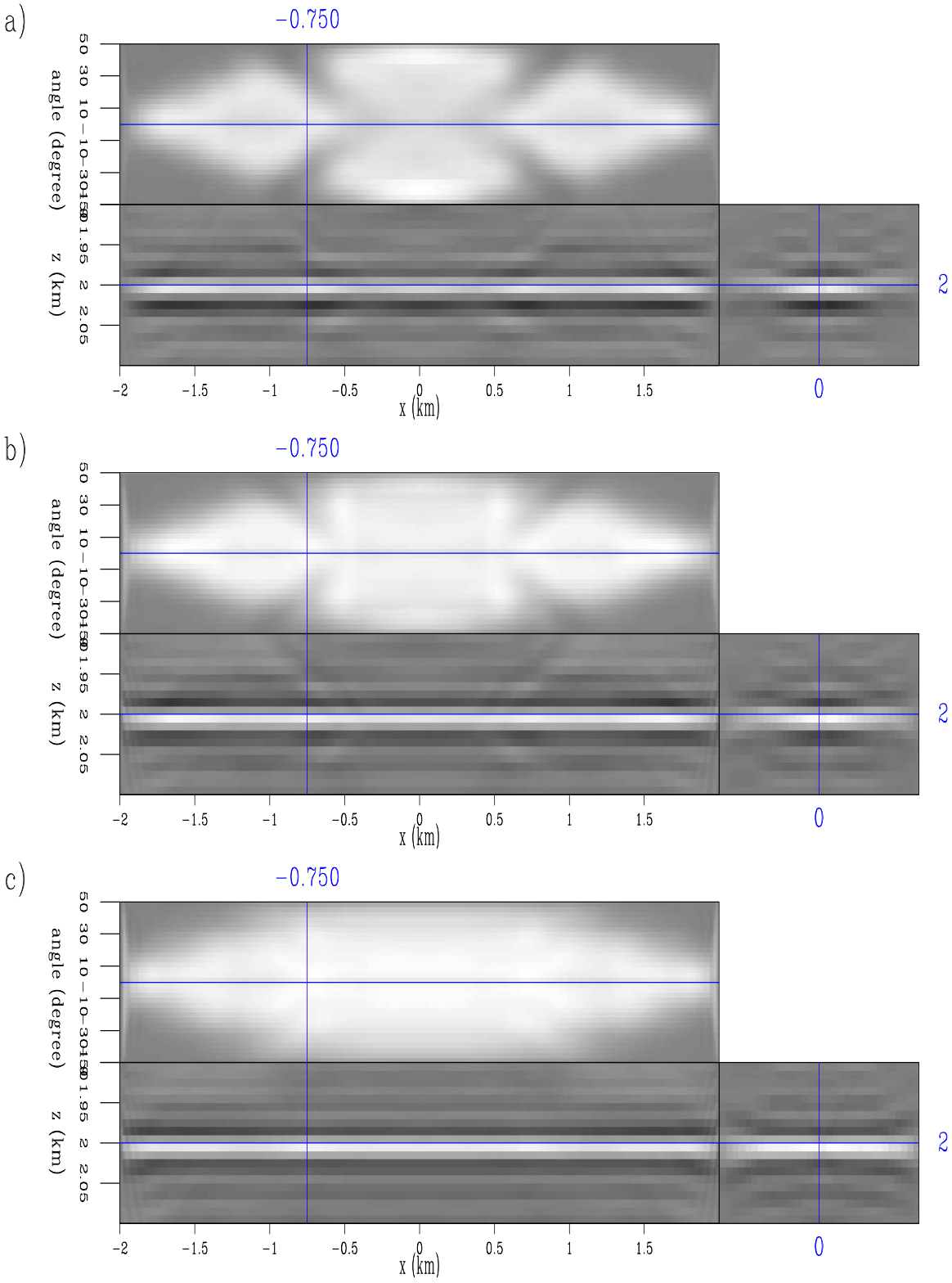

Figure 6: Comparison of the inversion results in reflection angle of the two-way (a) vs. the one-way modeled data (b), and vs. the migration "Hessian impulse response" (c) (from equation 3) alejandro1-compare_inv4 [CR,M]

affected by the velocity anomaly. Especially at the center of the model.

The results indicate that if the modeling and the inversion operators differ there is little chance to recover the correct AVA in poorly illuminated areas. This is because, in areas of poor illumination, this problem will have a large null space. The proper strategy appears to be the use of regularization. Three different regularization schemes for wave-equation inversion have been discussed in the literature. First, an identity operator (damping) which is customary in many scientific applications. Second, a geophysical regularization which penalizes the roughness of the image in the offset ray parameter dimension (which is equivalent the reflection angle dimension) (Prucha et al., 2000; Kuehl and Sacchi, 2001). Third, a differential semblance operator to penalize the energy in the image not focused at zero subsurface-offset (Shen et al., 2003).

CONCLUSIONS

Modeling and migration of a data set with a Gaussian velocity anomaly shows that the main differences between the two-way vs. one-way modeled data are at far offsets. The one-way modeled data amplitudes decay with offset, because of the many approximations used (PSPI to handle variable horizontal velocities) and the absence of the Jacobian of the change of variable from ω to k_z.

An important fact derived from the numerical experiments is that the one-way modeled data migration vs. migration "Hessian impulse response" show differences. Those differences are attributed to the computed number of off-diagonal terms of the Hessian matrix. An added value of this comparison is that it corroborates the approximations used to compute the Hessian.

The results indicate that if the modeling and the inversion operators differ there is little chance to recover the correct AVA in poor illumination areas. Because, in areas of poor illumination, this problem will have a large null space. The proper strategy to recover the AVA in those areas is the use of regularization, where previous knowledge about the model can be introduced to reduce the model null space.

ACKNOWLEDGMENTS

I would like to thank Bill Symes and TRIP for the Gaussian anomaly velocity model used in this paper.

REFERENCES

Claerbout, J. F., 1985, Imaging the earth's interior: Blackwell Scientific Publications.

Kuehl, H. and M. Sacchi, 2001, Generalized least-squares DsR migration using a common angle imaging condtion: Generalized least-squares DsR migration using a common angle imaging condtion:, Soc. of Expl. Geophys., 71st Ann. Internat. Mtg, 1025–1028.

Prucha, M. L., R. G. Clapp, and B. Biondi, 2000, Seismic image regularization in the reflection angle domain: SEP–**103**, 109–119.

Sava, P. and B. Biondi, 2001, Amplitude-preserved wave-equation migration: SEP–**108**, 1–26.

Sava, P. and S. Fomel, 2003, Angle-domain common-image gathers by wavefield continuation methods: Geophysics, **68**, 1065–1074.

Shen, P., W. Symes, and C. C. Stolk, 2003, Differential semblance velocity analysis by wave-equation migration: 73st Annual International Meeting, SEG, Expanded Abstracts, 2132–2135.

Tarantola, A., 1987, Inverse problem theory: Methods for data fitting and model parameter estimation: Elsevier Science Publication Company, Inc.

Valenciano, A. A. and B. Biondi, 2004, Target-oriented computation of the wave-equation imaging Hessian: SEP–**117**, 63–76.

Valenciano, A. A. and B. Biondi, 2006, Wave-equation angle-domain hessian: EAGE 68th Annual Conference, Expanded Abstracts.

Valenciano, A. A., B. Biondi, and A. Guitton, 2006, Target-oriented wave-equation inversion: Geophysics, **71**, no. 4, A35–A38.

Zhang, Y., G. Zhang, and N. Bleistein, 2005, Theory of true-amplitude one-way wave equations and true-amplitude common-shot migration: Geophysics, **70**, no. 4, E1–E10.